# Heterogenized Molecular Rhodium Phosphine Catalysts within Metal-Organic Frameworks for Alkene Hydroformylation

P. Samanta, A. Sole-Daura, R. Rajapaksha, F. Wisser, F. Meunier, Y. Schuurman, C. Sassoye, C. Mellot-Draznieks, J. Canivet

# Heterogenized Molecular Rhodium Phosphine Catalysts within Metal-Organic Framework for Alkenes Hydroformylation

Partha Samanta,[†] Albert Solé-Daura,[#] Remy Rajapaksha,[†] Florian M. Wisser,[Π] Frederic Meunier,[†] Yves Schuurman,[†] Capucine Sassoye,[⊥] Caroline Mellot-Draznieks[#] and Jerome Canivet[†,*]

[†] Univ. Lyon, Université Claude Bernard Lyon 1, CNRS, IRCELYON - UMR 5256, 2 Avenue Albert Einstein, 69626 Villeurbanne Cedex, France

[Π] Institute of Inorganic Chemistry, University of Regensburg, Universitätsstraße 31, 93053 Regensburg, Germany.

[⊥] Laboratoire de Chimie de la Matière Condensée de Paris (LCMCP), Sorbonne Université, UMR 7574 CNRS, Collège de France, 4 Place Jussieu, 75252 Paris Cedex, France.

[#] Laboratoire de Chimie des Processus Biologiques (LCPB), UMR CNRS 8229, Collège de France, PSL Research University, CNRS Sorbonne Université, 75231, Paris, France.

*Metal-organic Framework· Hydroformylation · Heterogeneous catalysis · Rhodium complex · Single-site catalyst*

**ABSTRACT:** Molecularly-defined organometallic rhodium phosphine complexes were efficiently heterogenized within a MOF structure without affecting neither their molecular nature nor their catalytic behavior. Phosphine-functionalized MOF-808 served as solid ligand in a series of eight rhodium phosphine catalysts. These MOF-heterogenized molecular catalysts showed activity up to 2100 $h^{-1}$ for ethylene hydroformylation towards propionaldehyde as sole carbon-containing product. Combined experimental and computational methods applied to this unique MOF-based molecular system allowed unravelling structure and evolution of the Rh active species within the MOF under catalytic conditions, in line with molecular mechanisms at play during the hydroformylation reaction. The MOF-based Rh catalyst also successfully catalyzed the hydroformylation of longer and bulkier alkenes with similar activity and selectivity than that obtained with its molecular homogeneous counterpart. The MOF-808 designed as a porous crystalline macroligand for well-defined molecular catalysts allows benefiting from molecular-scale understanding of interactions and mechanisms as well as from stabilization through site-isolation and recycling ability.

## INTRODUCTION

Homogeneous and heterogeneous catalysis are two essential keys to our industrialized society. These two processes reign supreme over the production of essential commodities while remaining impervious to each other. However, borders have to be crossed to generate breakthrough in the development of catalytic processes, including the design of novel catalytic species and the immobilization methodology on solid support, their combination being a powerful tool for a shift in paradigm in this field.[1–4] The design of novel heterogenized molecular catalysts should meet the needs of increased productivity compared to parent molecular analogues resulting from an enhanced stability allowing recycling while avoiding leaching of the active phase, with the necessary combination of high site density per catalyst mass or volume unit and high accessibility towards active sites.[5]

In this perspective, siliceous, purely organic or hybrid porous materials as supports have attracted special attentions for the design of single site heterogeneous catalysts by immobilizing molecular species.[6,7] Among these aforementioned porous solids, metal-organic frameworks (MOFs) have drawn intense research interest over the last few years due to their hybrid organic-inorganic nature associated with a high textural and chemical modularity.[8] Moreover, the MOF extended crystalline network allows for combining crystallographic techniques with computational studies to elucidate catalytic site nature and molecular catalytic mechanisms at play inside the porosity. [9–19]

In molecular catalysis, phosphines are widely used ligands whose both electronic and steric properties strongly influence the catalytic activity of the bound metal cation.[20] Phosphines have become essential to drive the catalytic activity and selectivity in applications ranging from fine chemistry with asymmetry and C-C coupling reactions, to petrochemistry with valorization of olefins using catalyzed oligomerization, hydroformylation, hydrogenation and metathesis.[21] In the case of hydroformylation reactions, the known deactivation of rhodium phosphine molecular catalysts by the formation of dinuclear species would be circumvented thanks to their irreversible single site isolation onto solid supports.[22]

Although MOFs have been employed as solid porous supports for molecular complexes in various catalytic applications,[23–25] MOFs based heterogeneous catalysts with well-defined and accessible free phosphine groups are still scarce.[26,27] The direct synthesis of phosphine-functionalized MOF (P-MOF) often led to phosphine oxidation within the MOF and subsequently to ill-defined sites for further metal cation coordination, as previously evidenced by solid-sate $^{31}$P NMR or X-ray absorption spectroscopy.[28–30] Without spectroscopic evidences, strictly inert atmosphere for both synthesis and metal coordination has been claimed to be mandatory for the successful preparation of oxide-free P-MOF catalysts,[31,32] leaching of the active metal being observed in some cases upon recycling.[33]

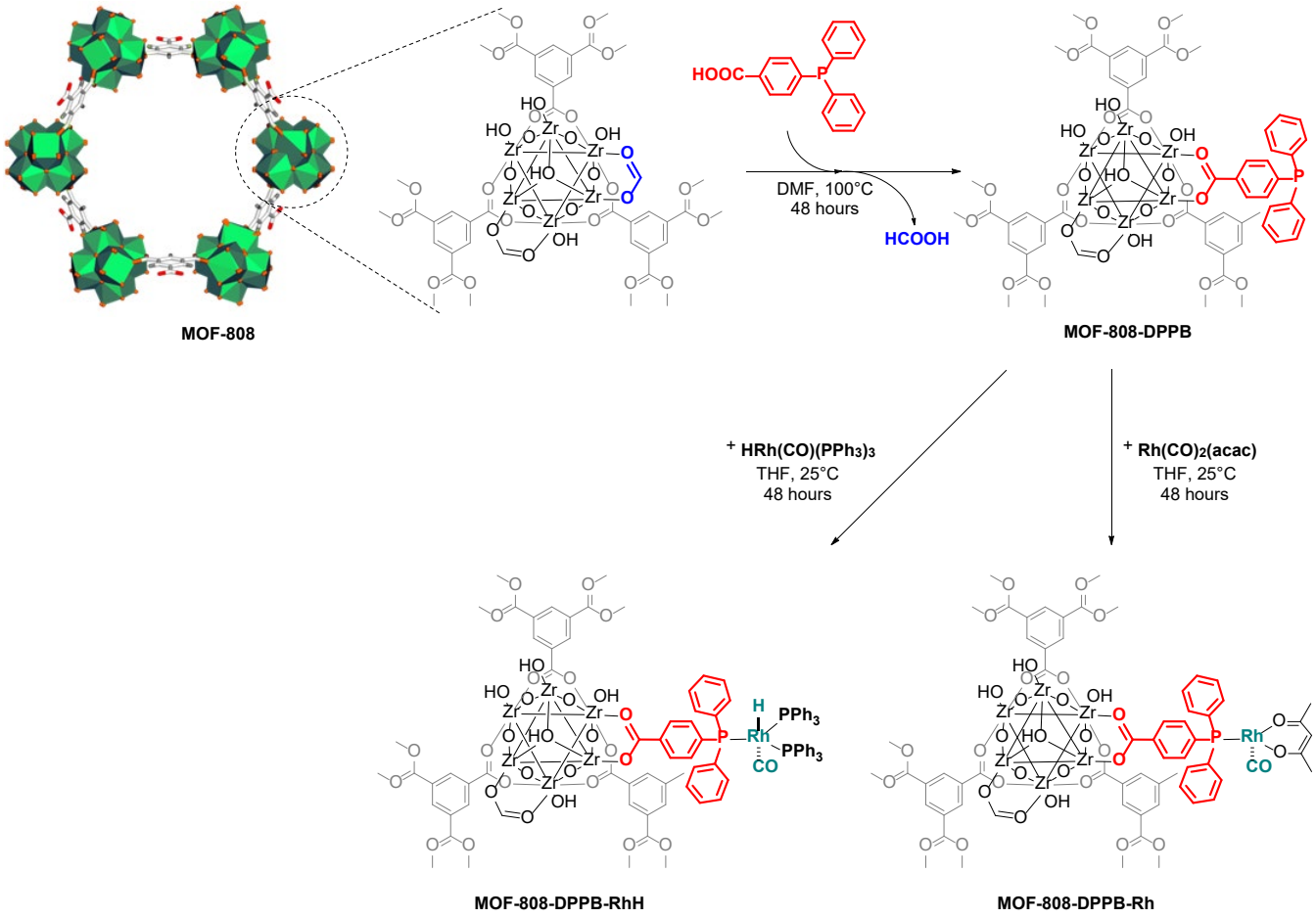


**Scheme 1. Rhodium phosphine molecular complexes assembly within MOF-808 porosity.**

In contrast to direct synthesis, a post-synthetic modification allows introducing a wide variety of functional groups without altering the structure of the MOF.[34–36] Wright, Clarke and coworkers already reported the post-synthetic grafting of sulfonated phosphine at the surface of the inorganic nodes of Hf-MOF, without oxidation, and its use as support for molecular iridium and rhodium catalysts, respectively for the reductive amination reaction and for the hydroaminomethylation of alkenes.[37]

Despite some achievements using non-covalently bonded Rh-based catalysts within MOF,[38–42] the use of covalently functionalized structures for the hydroformylation reaction remains restricted so far to N-coordinated Rh and Co single sites into a pyrazolyl-based MOF for the transformation of styrene.[43]

This irreversible heterogenization of well-defined molecular catalysts is a prerequisite to fully heterogeneous single-site catalysis. Such catalyst would benefit from recyclability, thus increasing the sustainability of the catalytic process, as well as molecular understanding of the catalyst behavior at the MOF interface, both remaining still to be demonstrated so far.

In this work, we report well-defined rhodium phosphine-functionalized MOFs able to promote the liquid-phase hydroformylation of $C_2$ to $C_{12}$ alkenes. We demonstrate the efficient and controlled phosphine ligand installation on the backbone of the MOF, to further fabricate Rh-based heterogeneous catalysts, by grafting the 4-(diphenylphosphino)benzoic acid (DPPB) on the secondary building unit (SBU) of a highly stable Zr-MOF without significant undesired oxidation (Scheme 1). Thanks to a combined experimental-computational approach, well-defined Rh(DPPB) complexes anchored inside the MOF cavity are demonstrated to retain their molecular nature and subsequently their molecular catalyst behavior while taking advantage of their heterogenization within a porous solid.

## RESULTS AND DISCUSSIONS

**Synthesis and characterizations of Rh@MOF-808 catalysts series.** Zirconium-based MOF-808 was chosen here as the targeted solid support for the synthesis of heterogeneous catalyst for hydroformylation reaction. MOF-808 has been discovered by Yaghi and co-workers[44] and further pioneered in different applications.[45–48] MOF-808 is built around $Zr_6O_4(OH)_6$ inorganic nodes connected by 1,3,5-benzenetricarboxylate (BTC) organic linkers to form a network of one-dimensional channels with pore size of 1.8 nm.[44] Although MOF-808 does not possess any direct functional groups, the possible installation of functional organic species at the second-

ary building unit by formate linker exchange has made it an attractive platform for molecular catalyst heterogenization.[49–51]

In this work, MOF-808 was synthesized by following a previously reported protocol by Yaghi and co-workers.[49] After the synthesis and solvent molecules removal by exchange and activation at 120°C under vacuum, the MOF was characterized by powder X-ray diffraction (PXRD), $N_2$ adsorption, elemental analysis, Fourier transform infrared (FT-IR), thermogravimetric analysis (TGA), transmission electron microscopy (TEM) microscopy etc. (see Supporting Information for details). The PXRD pattern of the synthesized MOF-808 was found to give a good match with those previously reported (Figure 1a). A Brunauer–Emmett–Teller (BET) surface area of 2282 $m^2g^{-1}$ was determined for MOF-808 from $N_2$ adsorption at 77 K (Table 1 and Figure S2). Also, a combined study of scanning electron microscopy (SEM) and transmission electron microscopy (TEM) revealed octahedral morphology for the MOF particles with an average size of 500-600 nm (Figures S3-S4).

The grafting of DPPB moiety inside MOF-808 was first carried out with desolvated MOF (250 mg) using 0.25 mmole of the aforementioned phosphine linker in dimethylformamide (DMF, see supporting Information for details). The phosphine-grafted material was washed with DMF and ethanol, and further activated at 120 °C under vacuum.

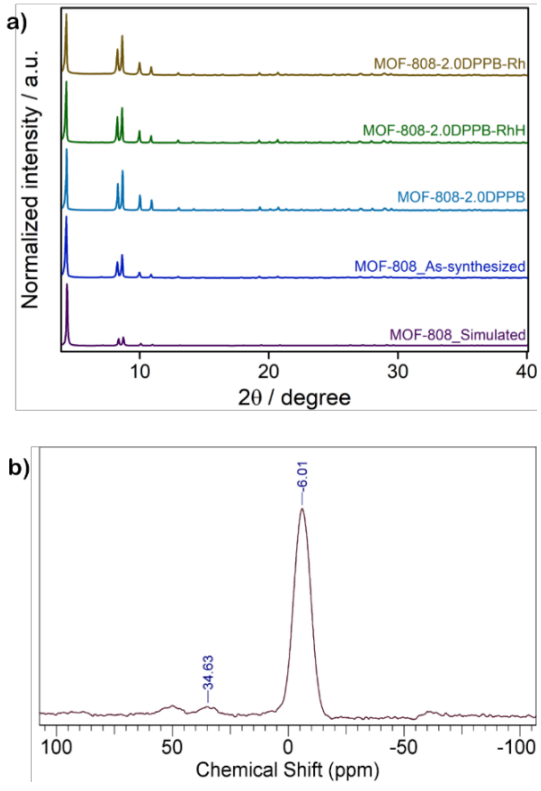


**Figure 1.** (a) Powder X-ray diffraction (PXRD) patterns of MOF-808 simulated from single crystal structure (purple), of as-synthesized MOF-808 (blue), of MOF-808-2.0DPPB upon DPPB grafting (cyan), and then upon $RhH(CO)(PPh_3)_3$ (green) and $Rh(CO)_2(acac)$ (dark yellow) infiltration, respectively. (b) Solid state $^{31}$P-NMR of MOF-808-2.0DPPB.

The amount of phosphorus was measured by ICP-OES to be around 2 wt% in the DPPB-functionalized MOF-808, which was named accordingly **MOF-808-2.0DPPB**.

The structural integrity of **MOF-808-2.0DPPB** was confirmed by PXRD (Figure 1a). The grafting of the DPPB occurs via linker exchange at the $ZrO_4(OH)_6$ node by replacing a formate with the carboxylate group of the DPPB molecule in an equimolar ratio (Figure S13). Moreover, the presence of phosphorus in the resulting material was confirmed by solid state $^{31}$P NMR analysis, with a peak at around -6.1 ppm corresponding to the dangling free phosphine, *ie.* without significant oxidation and non-coordinated to any metal (Figure 1b).

The FT-IR spectrum of **MOF-808-2.0DPPB** exhibits an additional peak at 1186 $cm^{-1}$, when compared to that of the parent MOF-808, which can be assigned to the stretching of P-phenyl rings (Figure S9), supporting its successful grafting. The octahedral morphology of the MOF-808 crystals was found to be retained from SEM and TEM analyses upon DPPB grafting (Figure S10-S11).

The ratio between the two organic units, BTC and DPPB, was also calculated from $^1$H NMR analysis of the MOF-808-2.0DPPB digested in HF and DMSO-$d_6$ solution (Figure S13). Both ICP-OES and $^1$H NMR analyses were found in line regarding the number of DPPB linkers, ca. 1.3 linkers grafted per node of MOF-808. A decrease of the surface area for **MOF-808-2.0DPPB** (1247 $m^2g^{-1}$) when compared to that of the parent MOF was observed and can be attributed to the inclusion of bulky DPPB linkers inside the porous network of MOF-808. (Table 1).

**Table 1. Textural properties of MOF-808 and respective derivatives**

| *Compound* | *DPPB per node* [a, b] | *Rh loading (wt%)* [b] | *Surface area ($m^2/g$)* [c] |
|---|---|---|---|
| MOF-808 | *0* | *0* | *2282* |
| MOF-808-0.9DPPB | *0.4* | *0* | *1826* |
| MOF-808-0.9DPPB-Rh | *0.4* | *0.83* | *1694* |
| MOF-808-0.9DPPB-RhH | *0.4* | *0.79* | *1576* |
| MOF-808-2.0DPPB | *1.3* | *0* | *1247* |
| MOF-808-2.0DPPB-Rh | *1.3* | *0.72* | *977* |
| MOF-808-2.0DPPB-RhH | *1.3* | *0.62* | *852* |
| MOF-808-3.1DPPB | *2.5* | *0* | *709* |
| MOF-808-3.1DPPB-Rh | *2.5* | *0.63* | *662* |
| MOF-808-3.1DPPB-RhH | *2.5* | *0.56* | *594* |
| MOF-808-3.7DPPB | *3.3* | *0* | *466* |
| MOF-808-3.7DPPB-Rh | *3.3* | *0.54* | *326* |
| MOF-808-3.7DPPB-RhH | *3.3* | *0.48* | *318* |
| MOF-808-Rh | *0* | *1.0* | *308* |
| MOF-808-RhH | *0* | *0.73* | *283* |

[a] determined by $^1$H NMR analysis, [b] determined by ICP-OES analysis, [c] determined from nitrogen physisorption measurement at 77K using BET method.

The postulated molecular formula of the **MOF-808-2.0DPPB** was calculated based on elemental analysis, ICP-OES, and NMR spectroscopy to give $Zr_6O_4(OH)_6(C_9H_3O_6)_2(HCOO)_{2.7}(C_{19}H_{15}O_2P)_{1.3}(DMF)_{1.5}$.

To gain more insight on the influence of the phosphine concentration inside the framework on both the active metal coordination at the phosphine site and the subsequent catalytic activity of the respective materials, we varied the amount of DPPB linkers grafted inside MOF-808. A series of DPPB-grafted MOF materials have been synthesized by varying the amount of DPPB from 0.1 to 2 mmol (in total 0.1, 0.25, 0.5, 1.0 and 2.0 mmol, respectively) during the grafting process. The structural integrity of these post-synthetically modified materials was found to be retained according to PXRD analysis (Figure S14). From ICP-OES measurements, the loading of phosphorus for these additional materials was found to be 0.9 wt%, 3.1wt%, 3.1 wt% and 3.7 wt% of phosphorus for the 0.1, 0.5, 1.0 and 2.0 mmol of linkers used for the grafting, respectively. Since the use of 0.5 and 1.0 mmol of linkers during post-modification have led to a similar amount of phosphine grafted into the MOF-808, the material synthesized from 1.0 mmol of phosphine was excluded from further studies. In addition to **MOF-808-2.0DPPB**, according to the loading in mass of phosphorus, the three additional aforementioned materials were named as **MOF-808-0.9DPPB**, **MOF-808-3.1DPPB** and **MOF-808-3.7DPPB**, respectively. Accordingly, the number of DPPB linkers per SBU was estimated for **MOF-808-0.9DPPB**, **MOF-808-3.1DPPB** and **MOF-808-3.7DPPB** to be 0.4, 2.5 and 3.3 respectively (Table 1). To further confirm the number of DPPB grafted in MOF-808, liquid state $^1$H NMR analyses have been performed for the aforementioned compounds after digestion in HF and DMSO-$d_6$ (Figures S16-S18). The number of grafted phosphines in the respective materials calculated from $^1$H NMR was found to be in line with the number of DPPB per SBU obtained from ICP-OES. Nitrogen physisorption measurements were carried out at 77 K to assess the porosity of the DPPB-grafted materials. (Figure S15). Again, with increasing amount of bulky DPPB dangling moieties inside MOF-808, the $N_2$ uptake was found to decrease along with the BET surface area and the total pore volume (Table 1). Moreover, solid state $^{31}$P-NMR measurements for all these materials have revealed a negligible amount of oxidation on the phosphorus sites which thus remain readily available for further metalation (Figures S19-S21).

In a second step, the DPPB-grafted MOF-808 materials were subjected to metalation, using either $RhH(CO)(PPh_3)_3$ or $Rh(CO)_2(acac)$ (acac : acetylacetonate) as metal precursors, to obtain the MOF-808-DPPB-RhH and MOF-808-DPPB-Rh series, respectively (Scheme 1).

The ability to heterogenize Rh-P species within the MOF cavity is demonstrated here for the first time on the **MOF-808-2.0DPPB** solid. The structural integrity of **MOF-808-2.0DPPB-RhH** and **MOF-808-2.0DPPB-Rh** was found to be retained according to PXRD analysis (Figure 1a). The amount of rhodium in both catalysts was determined by ICP-OES analysis, yielding a rhodium loading of 0.62 and 0.72wt% for **MOF-808-2.0DPPB-RhH** and **MOF-808-2.0DPPB-Rh**, respectively (Table 1). Moreover, a shift in solid state $^{31}$P-NMR spectra was observed for the both Rh infiltrated materials. The peak at -6.0 ppm in the $^{31}$P NMR spectrum for the **MOF-808-2.0DPPB** was found to be partially shifted to 32.9 ppm for **MOF-808-2.0DPPB-RhH** with an additional peak at ca. 37.3 ppm attributed to additional Rh-coordinated $PPh_3$, while shifted to 32.3 ppm for **MOF-808-2.0DPPB-Rh** (Figures S24-S25). The respective molecular formulas for these catalysts have been determined according to elemental analysis, ICP-OES, and $^1$H and $^{31}$P NMR spectroscopies. The proposed molecular formula of **MOF-808-2.0DPPB-RhH** is $Zr_6O_4(OH)_6(C_9H_3O_6)_2(C_{19}H_{15}O_2P)_{1.3}(HCOO)_{2.7}[RhH(CO)(PPh_3)_2]_{0.13}$, and that of **MOF-808-2.0DPPB-Rh** is $Zr_6O_4(OH)_6(C_9H_3O_6)_2(C_{19}H_{15}O_2P)_{1.3}(HCOO)_{2.7}[Rh(CO)_2(C_5H_7O_2)]_{0.14}$.

On the other hand, the peak at 1186 cm$^{-1}$ (C-H stretching of P-phenyl ring) in FT-IR spectrum of MOF-808-2.0DPPB has been found to be weaker in the spectrum recorded after Rh loading of MOF-808-2.0DPPB, which might be attributed to the binding of the phosphines to the Rh cations (Figure S26).

Finally, according to SEM and TEM analysis, the octahedron morphology of the MOF-808 particles was found to be retained after Rh precursor infiltration and no Rh aggregates have been observed (Figure S28-S31).

The actual coordination of the rhodium towards dangling phosphine atoms within the MOF cavity as well as the molecular nature of the Rh-P catalyst being assessed, the same methodology has been applied to the whole DPPB-grafted MOF-808 series.

The obtained new six catalysts were named according to the mass loading (wt%) of phosphorus and the nature of the rhodium precursor: $RhH(CO)(PPh_3)_3$ has led to **MOF-808-0.9DPPB-RhH**, **MOF-808-3.1DPPB-RhH** and **MOF-808-3.7DPPB-RhH**; while **MOF-808-0.9DPPB-Rh**, **MOF-808-3.1DPPB-Rh** and **MOF-808-3.7DPPB-Rh** were obtained using $Rh(CO)_2(acac)$. According to PXRD analyses, the structural integrity of these catalysts has been maintained similar to that of the parent MOF-808 (Figure S34-S35). All the aforementioned six MOF-808 based catalysts have been found to be retained substantial amount of porosity even after the infiltration of Rh metal inside the porous architecture of the MOF-808. The apparent surface areas in these materials decrease with increasing amount of linkers grafted to MOF-808 (Table 1). ICP-OES analyses have provided the amount of Rh infiltrated in respective catalysts (Table 1). It can be stated that with the higher amount of DPPB linkers inside MOF-808 the extent of Rh infiltration has got reduced slightly. This result can be attributed to the pore blocking effect of bulky DPPB linkers which have opposed the effective diffusion of the respective Rh precursors into the porous channels of MOF-808. For the set of catalysts obtained from $RhH(CO)(PPh_3)_3$ precursors, the wt % of Rh have been found to be 0.79, 0.62, 0.56 and 0.48 for **MOF-808-0.9DPPB-RhH**, **MOF-808-2.0DPPB-RhH**, **MOF-808-3.1DPPB-RhH** and **MOF-808-3.7DPPB-RhH,** respectively (Table 1). The ratio of linker to Rh (DPPB:Rh) have been calculated from aforementioned data and which have been 4:1, 11:1, 18:1 and 25:1 for **MOF-808-0.9DPPB-RhH**, **MOF-808-2.0DPPB-RhH**, **MOF-808-3.1DPPB-RhH** and **MOF-808-3.7DPPB-RhH,** respectively. On the other hand, catalysts obtained from $Rh(CO)_2(acac)$ precursors, the wt % of Rh have been found to be 0.83, 0.72, 0.63 and 0.54 for **MOF-808-0.9DPPB-Rh,**

**MOF-808-2.0DPPB-Rh, MOF-808-3.1DPPB-Rh** and **MOF-808-3.7DPPB-Rh**, respectively (Table 1). Again, the linker to Rh ratio (DPPB:Rh) have been calculated to be 4:1, 9:1, 16:1 .and 23:1 for **MOF-808-0.9DPPB-Rh**, **MOF-808-2.0DPPB-Rh**, **MOF-808-3.1DPPB-Rh** and **MOF-808-3.7DPPB-Rh,** respectively.

**Molecular structure of heterogenized catalysts.** In order to get further insight into the atomic-level structure of the phosphine-grafted MOF-808 and the heterogenized Rh complexes, a computational chemistry approach including force-field based simulations and density functional theory (DFT)-level calculations was conducted (see Supporting Information for computational details). In a first step, relying on the experimental phosphorus content in **MOF-808-2.0DPPB** and the reported X-ray crystal structure of MOF-808 ,[44] we realized the *in silico* functionalization of the cubic unit cell of MOF-808 with 21 DPPB molecules by means of sequential forcefield-based Monte Carlo (MC) docking and Molecular Dynamics (MD) simulations (see Supporting Information for computational details). Either in the docking steps or in subsequent MD equilibration steps, all phosphines were indeed found to simultaneously interact with two neighboring Zr atoms of a $Zr_6$-oxocluster through their carboxylate groups (Figure S79).

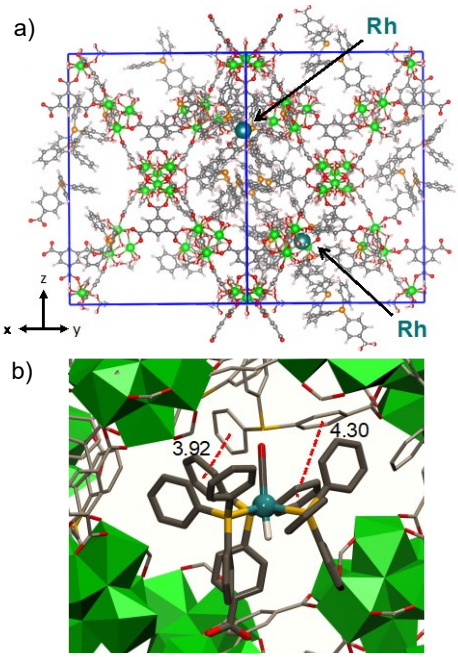


**Figure 2.** Computed model of **MOF-808-2.0DPPB-RhH** catalyst from force field-based MC/MD simulations. a) 3D-periodic cubic cell of MOF-808 containing 21 DPPB and 2 Rh-hydrido precursors coordinated to one grafted phosphine each. The two Rh centers installed in the unit-cell are highlighted as cyan spheres. b) Detailed view of one of the grafted Rh-hydrido catalyst precursors, where van der Waals interactions between phenyl rings are tracked by measuring distances between their centroids (red dashed lines). Distances are given in Å and C-bound H atoms are omitted for clarity. Color code: Zr (green), Rh (cyan), P (orange), C (gray), O (red), H (white).

In a second step, using a similar force field-based MC/MD computational strategy than above and in line with the experimental Rh-loading in **MOF-808-2.0DPPB-RhH** (P : Rh = 21 : 2), two molecular Rh precursors were installed in the unit cell of the DPPB-functionalized MOF in the form of $RhH(CO)(PPh)_2$ species, the Rh center lacking one of its $PPh_3$ ligands thus allowing for a possible additional coordination to a dangling MOF-grafted phosphine (Figure 2a). In the resulting model of **MOF-808-2.0DPPB-RhH**, the two Rh centers were indeed found to sit on one MOF-grafted phosphine each, leading to $RhH(CO)(PPh)_2(DPPB)$ species. The Rh molecular complexes are not only attached to the MOF through direct Rh-P bond but also stabilized via van der Waals interactions with free neighboring grafted phosphines (Figure 2b).

The same type of interactions was found when refining the proposed structure of **MOF-808-2.0DPPB-RhH** with periodic DFT-D3 level calculations using a smaller primitive cell, further validating the employed methodology (Figure S80).

Prompted by the observed proximity between the fully coordinated $RhH(CO)(PPh)_2(DPPB)$ species and other grafted DPPB within the same pore, we explored whether more than one $PPh_3$ ligand remaining at the Rh center could be further exchanged with one MOF-grafted DPPB. To this end, DFT calculations at the ωB97X-D level and including solvent effects were conducted on cluster models extracted from the periodic systems described above. These calculations predict that the conformation in which the Rh keeps two initial $PPh_3$ ligands and coordinates to only one MOF-grafted DPPB is slightly more thermodynamically favorable (by 13 kJ/mol) than the binding to two DPPB from the MOF (Scheme S5). However, both of them might coexist in the MOF due to their small free-energy difference. The same approach was used to study the grafting of the Rh(acac) precursor into the DPPB-grafted MOF while exploring four different binding modes. More specifically, we analyzed the possible replacement of a CO or one of the oxygens of the acac ligand by a DPPB, exploring for the latter its binding to both an axial or an equatorial position at the Rh site (Scheme 2 and see Supporting Information for computational details).

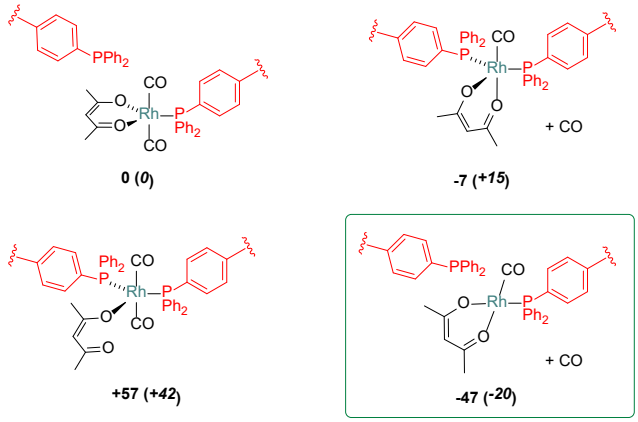


**Scheme 2.** Various binding modes for the Rh-acac precursor studied inside the pores of the phosphine-modified MOF-808. Relative Gibbs free energies and relative enthalpies (italics, in parentheses) are given in kJ/mol.

In the **MOF-808-2.0DPPB-Rh**, the most stable complex conformation involved a square-planar Rh center coordinated to the pristine acac ligand, one CO and one MOF-grafted DPPB (Scheme

2, green frame). Again, the coordination of the Rh center by two DPPB at MOF-808 was found to be less energetically favorable.

Overall, the above theoretical calculations support that the Rh phosphine catalysts can be efficiently heterogenized within the phosphine-grafted MOF-808, whereby the key molecular features of their coordination environment required to be catalytically active are preserved. The MOF-808-DDPB acts as a solid reservoir of phosphines whose site isolation allows for the generation of active carbonyl rhodium phosphine complexes without reaching the saturation of the Rh coordination sites with excess phosphines in its environment, in contrast to phenomena observed in solution where excess phosphines led to inactive Rh species.[52]

Pair distribution function (PDF) analysis was used to further get experimental insight into MOF-based catalyst structure by ways of inter-atomic distances, relying on the above computed models of **MOF-808-2.0DPPB** and **MOF-808-2.0DPPB-Rh** (see Supporting Information for details). This technique has been already shown to be applicable even to amorphous MOF materials[53] and has been recently successfully used to assess the structural integrity of MOF-supported polyoxometalate catalysts [54] as well as Rh active sites in MOP-based materials.[55] It has also been recently used to detect highly loaded single site metals trapped by catechol-benzoate ligands into MOF-808 (approx. 0.3-0.4 Fe or Cu per Zr).[56] Here, our PDF analysis of MOF-808-funtionalized solids showed, as seen by XRD, that the MOF-808 long range ordered structure is preserved upon both DPPB and Rh species functionalization (see Supporting Information). Despite a low complex loading within the MOF (approx. 0.2 Rh per Zr), small differences are observed between experimental *G(r)* curves at low range order (from **MOF-808** to **MOF-808-2.0DPPB**, **MOF-808-2.0DPPB-RhH** and **MOF-808-2.0DPPB-Rh**, see Figures S76-S77). We interpreted those small modifications as a signature of the grafting of the phosphine ligand (with P-C distances responsible of a shoulder at 2.75 Å) and Rh-P coordination. Moreover, a slight $Zr_6$ node local modification can be observed and attributed to a small distortion of the $Zr_6(\mu_3\text{-}O)_4(\mu_3\text{-}OH)_4(\mu1\text{-}OH)_2(\mu1\text{-}H_2O)_2(HCOO)_4$ node geometry as a consequence of the grafting of DPPB, and subsequent Rh coordination, replacing the more flexible formate moieties, while maintaining the $Zr_6$ node's size and connectivity to BTC linkers.

**MOF-catalyzed ethylene hydroformylation.** The obtained series of MOF-based heterogeneous catalysts were first evaluated in the ethylene hydroformylation towards propionaldehyde. The increasing availability of ethylene from shale gas[57] and bioethanol[58] makes appealing its conversion into value-added chemicals and propionaldehyde produced from hydroformylation can be further converted into propylene,[59] having a pivotal role in polymer industry.

In order to verify the role of grafted DPPB ligands in MOF-808 in catalysis, MOF based catalysts without DPPB and impregnated with Rh precursors were synthesized as well. **MOF-808-RhH** and **MOF-808-Rh** were synthesized from $RhH(CO)(PPh_3)_3$ or $Rh(CO)_2(acac)$ respectively, and further characterized with PXRD, ICP-OES and nitrogen physisorption. PXRD patterns of the respective catalysts confirmed the retention of the structural integrity after the infiltration of respective Rh salts (Figures S40 and S43). The ICP-OES measurements showed the presence of physisorbed Rh species with loading of 0.73 and 1.0 wt% in **MOF-808-RhH** and **MOF-808-Rh,** respectively.

The early reaction conditions have been defined to be 20 bars of continuous feed of a 1:1:1 mixture of $C_2H_4$:CO:$H_2$ using toluene as solvent at 110 °C in order to give reasonably high catalytic activity in triphasic batch reactor (Table 2). After completion, reactions were analyzed by gas chromatography (GC) of the liquid phase. The turn over numbers (TON) were calculated from product yield with respect to internal standard (dodecane). It is worthy to note that all catalytic systems selectively produced propionaldehyde as sole carbon-containing product. Indeed, GC analysis of the gaseous phase, using head-space sampler, confirmed the absence of ethane or $CO_2$ in the reaction mixture, whereas the formation of propanol was ruled out from the GC analysis of the reaction solution. The performances of **MOF-808-2.0DPPB-RhH** and **MOF-808-2.0DPPB-Rh** (Table 2, entries 1-2) were compared with those of their homogeneous analogues (Table 2, entries 5-10). Catalytic conversion of ethylene with **MOF-808-2.0DPPB-RhH** led to a TON of 4413. Moreover, the other heterogeneous catalyst, **MOF-808-2.0DPPB-Rh,** led to a TON of 2268.

**Table 2. Catalytic activity of MOF-808-derived catalysts in ethylene hydroformylation compared to their homogeneous analogues.[a]**

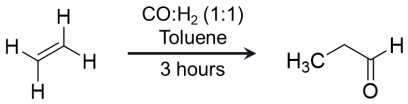


| Entry | Catalyst | TON [b] | TOF [c] |
|---|---|---|---|
| 1 | *MOF-808-2.0DPPB-RhH* | *4413* | *1471* |
| 2 | *MOF-808-2.0DPPB-Rh* | *2268* | *756* |
| 3 | *MOF-808-RhH* [d] | *2169* | *723* |
| 4 | *MOF-808-Rh* [e] | *1507* | *502* |
| 5 | *$RhH(CO)(PPh_3)_3$* [f] | *3235* | *1078* |
| 6 | *$RhH(CO)(PPh_3)_3$ + DPPB* [f,g] | *2237* | *746* |
| 7 | *$RhH(CO)(PPh_3)_3$ + $PPh_3$* [f,g] | *2773* | *924* |
| 8 | *$Rh(CO)_2(acac)$* [f] | *2435* | *812* |
| 9 | *$Rh(CO)_2(acac)$ + DPPB* [f,g] | *3502* | *1167* |
| 10 | *$Rh(CO)_2(acac)$ + $PPh_3$* [f,g] | *2287* | *762* |

[a] Reaction conditions: 10 mg of solid catalysts (heterogenous) were used with Rh amount of 0.6-0.7 μmol; 110°C temperature, 20 bar constant pressure of a 1:1:1 mixture of $C_2H_4$:CO:$H_2$, 20 mL toluene, 80 μL dodecane as internal standard; reaction time 3 hours; [b] turn over number (TON) was calculated from GC analysis and defined as moles of propionaldehyde produced per mole of Rh; [c] turn over frequency (TOF) defined as moles of propionaldehyde formed per moles of Rh per hour determined after 3 hours of reaction; [d] 0.65 μmol of Rh; [e] 0.7 μmol of Rh; [f] Homogeneous analogous reactions; [g] 1:1 mixture of Rh precursors and respective linkers (0.6-0.7 μmol).

Homogeneous Rh precursors alone and along with an equimolar mixture of DPPB and $PPh_3$ were tested (Table 2, entries 5-7). The

homogeneous $RhH(CO)(PPh_3)_3$ analogous catalyst showed a slightly lower catalytic activity compared to that of **MOF-808-2.0DPPB-RhH** with a TON of 3235 after 3 hours. The TON obtained for an equimolar mixture of $RhH(CO)(PPh_3)_3$ and DPPB or $PPh_3$ was found to be 2237 and 2773, respectively, lower than that of the corresponding heterogeneous catalyst **MOF-808-2.0DPPB-RhH**. In this case, the higher propionaldehyde production with the **MOF-808-2.0DPPB-RhH** compared to homogeneous analogues might arise from stabilizing interactions between the MOF-grafted DPPB and Rh-coordinated phosphines (Figure 2b). Other homogenous analogous catalyst $Rh(CO)_2(acac)$ showed comparable activity with TON up to 3502 in the presence of DPPB as additive (Table 2, entries 8-10), higher than that of the heterogeneous counterpart **MOF-808-2.0DPPB-Rh** (Table 2, entries 2). This might be attributed to the easier and faster formation of the RhH(CO) active species from Rh(acac) in solution, according to hydroformylation reaction mechanism,[60,61] in contrast to the analogous species grafted within the constrained environment of the MOF cavity.

To validate the role of grafted DPPB in **MOF-808-DPPB**-based catalysts, phosphine-free impregnated **MOF-808-Rh** and **MOF-808-RhH** were employed under the same catalytic conditions (Table 2, entries 3-4). The formation of propionaldehyde from ethylene was found to take place with TON of 2169 and 1507 for **MOF-808-RhH** and **MOF-808-Rh**, respectively. The higher efficiency of **MOF-808-2.0DPPB-Rh** and **MOF-808-2.0DPPB-RhH** can be attributed to the well-defined active catalytic sites which are coordinated by DPPB inside pores of **MOF-808**. Furthermore, ICP-OES analysis revealed a massive leaching of Rh in the case of DPPB-free **MOF-808-RhH** and **MOF-808-Rh** catalysts (Table S5). The optimization of the DPPB loading within MOF-808, and the subsequent phosphine-to-rhodium ratio, was then investigated. All the eight catalysts obtained from two different Rh precursors and varied DPPB ligand have been tested for hydroformylation of ethylene using the same condition as earlier at 110 °C and 20 bar pressure for 3 hours (Figure 3). As shown in Figure 3a, in the case of the four catalysts obtained from $RhH(CO)(PPh_3)_3$, an initial increase in catalytic activity was observed with increasing DPPB loading from 0.4 linkers per SBU (**MOF-808-0.9DPPB-RhH**) to 1.3 linkers per SBU (**MOF-808-2.0DPPB-RhH**). The corresponding TON for **MOF-808-0.9DPPB-RhH** catalyst has been found to be 1495, while it reached 4413 for **MOF-808-2.0DPPB-RhH**. Upon further increase in the DPPB linkers loading, a decrease in the TON was observed which might be attributed to an increased steric hindrance within the pores. As shown in Figure 3b, a less pronounced but similar trend was found for the other set of catalysts obtained from $Rh(CO)_2(acac)$. Thus, a maximum efficiency for the catalytic conversion of ethylene to propionaldehyde has been obtained with an optimum 1.3 DPPB linkers per SBU of MOF-808 for the both two series of catalysts.

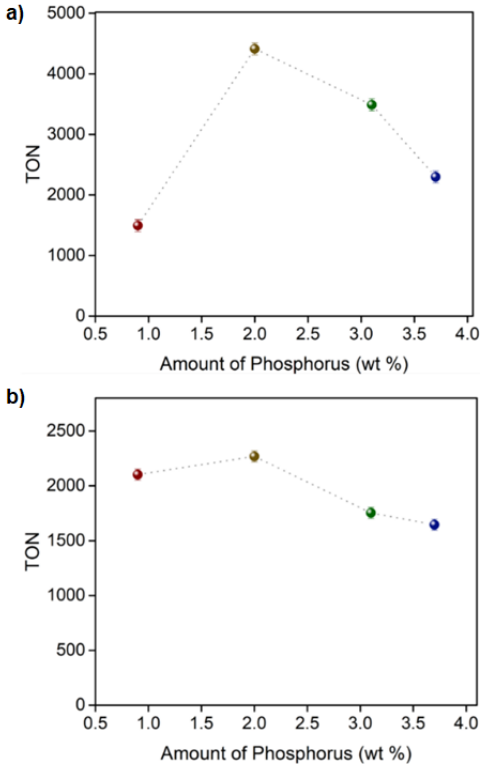


**Figure 3.** Catalytic activity of MOF-808 functionalized with various amount of DPPB linker and using (a) $RhH(CO)(PPh_3)_3$ or (b) $Rh(CO)_2(acac)$ as catalyst precursors. Reaction conditions: 10 mg of solid catalyst have been used corresponding to ca. 0.7 µmol of Rh; 110°C temperature, 20 bar pressure of a 1:1:1 mixture of $C_2H_4$:CO:$H_2$ and 20 mL toluene, 80 µL dodecane as internal standard; for 3 hours.

The kinetic profile obtained for the best performing heterogeneous catalyst, **MOF-808-2.0DPPB-RhH**, showed a constant and linear production of propionaldehyde for 3 hours which then slowed down slightly (Figures S57 and S58). This modification of reaction kinetics might be caused by an inhibition of active site in line with the increased propionaldehyde concentration, as previously reported for homogeneous counterparts,[62,63] and a change in the concentration of gaseous substrates dissolved in the solvent. After 24 hours of reaction, a change of the reactor head-space for fresh gaseous feed allowed the reaction to restart with similar initial activity (TOF = 1062 $h^{-1}$ calculated after 2 hours), highlighting the limitation due to change in reactant concentration in the closed vessel upon propionaldehyde production after 3 hours at 110°C and 20 bars (Figure S58). This evidenced the long-term stability of the catalyst under reaction conditions and allowed us to determine the intrinsic activity of the MOF-heterogenized Rh catalysts as turn over frequencies (TOF) defined as moles of propionaldehyde produced per moles of Rh per hours after 3 hours of reaction (Table 2).

To further assess the stability of the heterogeneous catalyst, thorough characterizations of both spent **MOF-808-2.0DPPB-RhH** and **MOF-808-2.0DPPB-Rh** have been carried out. The structural integrity for both catalysts was preserved according to PXRD analysis (Figure S61 and S67). The apparent surface area has been found to be retained (Figures S62 and S68). Also, TEM and SEM analysis

showed that the octahedral morphology of the catalyst crystals has been preserved after catalysis, without formation of Rh particles (Figure S63-S64 and S69-S70). Retention of Rh inside the MOF materials was confirmed by ICP-OES analysis (0.55 and 0.67 wt% for **MOF-808-2.0DPPB-RhH** and **MOF-808-2.0DPPB-Rh** respectively). XPS analysis revealed that no profound change in Rh oxidation state occurred (Figures S65-S66 and S71-S72).

The recyclability of the **MOF-808-2.0DPPB-RhH**, selected as best performing catalyst, was also evaluated for 3 hours of reaction (Figures 4 and S60). In this case, the reactor has been pressurized with the gas mixture at 20 bars and the pressure maintained constant. The **MOF-808-2.0DPPB-RhH** was found to reach similar catalytic activity for five consecutive runs. A leaching of rhodium in solution was evidenced by ICP-OES analysis after the first catalytic run, linked to a slight decrease in activity (Table S5). Hot filtration test showed however that no catalytically active species were present in solution during catalysis (Figure S59). Furthermore, no additional leaching was observed during the four subsequent catalytic runs (Table S5). Thus, after five catalytic runs of 3 hours, **MOF-808-2.0DPPB-RhH** allowed to reach a cumulative TON of ca. 21000 for the production of propionaldehyde, with a stable TOF of ca. 1400 $h^{-1}$ for each run at 110°C under 20 bars. In contrast, the use of **MOF-808-RhH**, in which Rh sites are most likely physisorbed at the surface and pores of the MOF in the absence of phosphine ligand, led to a drastic decrease in catalytic activity upon reuse and a massive leaching of rhodium in solution (Figure 4 and Table S5).

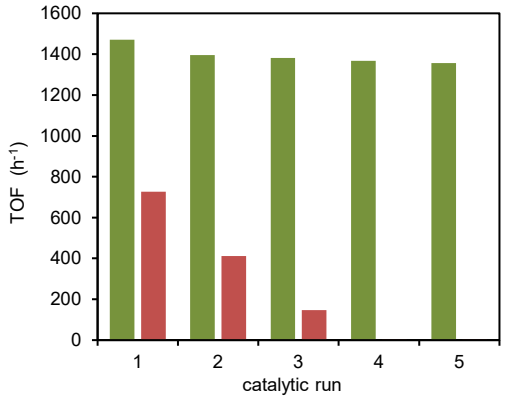


**Figure 4.** Catalyst recycling using **MOF-808-2.0DPPB-RhH** (green) and **MOF-808-RhH** (red, MOF without grafted DPPB) under 20 bar pressure, at 110 °C after 3 hours; pressure has been maintained constant.

To the best of our knowledge, we report here the first example of ethylene hydroformylation catalyzed by well-defined MOF-supported molecular catalysts.

For comparison, heterogenous organic polymer-supported Rh catalysts have been reported for the hydroformylation of ethylene. Under gas phase conditions, a phosphine-functionalized polystyrene loaded with Rh precursors show TON of 109 at 110 °C and 5 bar pressure of an equimolar mixture of $CO/H_2/C_2H_4$ after 20 hours.[64] More recently, another phosphine- based polymer along with the same Rh precursors has demonstrated very high activity under similar fixed-bed conditions with TOF up to 10000 $h^{-1}$ for a Rh loading as low as 0.063 wt% within the polymer.[65] However, despite appealing activities reported here with **MOF-808-DPPB-Rh** catalysts for liquid phase application, the transfer from triphasic batch to fixed-bed gas-phase reactor require the formulation and the shaping of the MOF catalysts into adequate bodies which are not trivial and are still under investigations.[66–69]

**Molecular-level comparison of the two MOF-808-DPPB-Rh systems.** In order to further investigate the catalytic behavior of the MOF catalysts made from the two different Rh precursors, we scrutinized the effect of both the pressure and the temperature on the catalytic activity using the two **MOF-808-2.0DPPB-RhH** and **MOF-808-2.0DPPB-Rh** catalysts (Figure 5). As expected, in the two cases, the activity increased with both the pressure of the gas feed and the temperature. Under the conditions used here, ethylene was still selectively converted into propionaldehyde. From temperature studies, it was observed that there was no catalytic activity at 30 °C with any of the catalysts even at 20 bar pressure. At 50°C and above, with increasing pressure from 5 bar to 20 bar at a fixed temperature the catalytic activity increased significantly. The catalytic activity reached a maximum for both catalysts at 125 °C and 20 bar pressure of gas feed with TON of 6342 and 5483 and initial TOF of 2114 $h^{-1}$ and 1828 $h^{-1}$ for **MOF-808-2.0DPPB-RhH** and **MOF-808-2.0DPPB-Rh**, respectively.

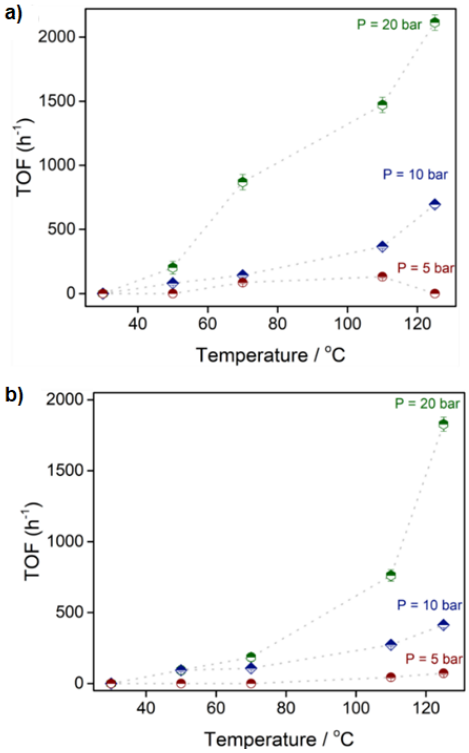


**Figure 5**. Temperature-dependent catalytic activity at varied pressure of gas mixture ($C_2H_4$:CO:$H_2$= 1:1:1) for (a) **MOF-808-2.0DPPB-RhH** and (b) **MOF-808-2.0DPPB-Rh**. All the reactions have been carried out in 20 mL toluene with 80 µL dodecane as internal standard and analyzed by GC.

The most significant difference in initial activity between the **MOF-808-2.0DPPB-RhH** and **MOF-808-2.0DPPB-Rh** appeared under 20 bars between 50 and 110°C where the catalyst

prepared from RhH precursor showed a twice higher TOF than its Rh(acac) counterpart. Indeed, the comparison of the evolution of the propionaldehyde production for the two MOF-based systems during 24 hours, at 110°C under 20 bars, highlighted a lower initial activity for the **MOF-808-2.0DPPB-Rh** compared to the **MOF-808-2.0DPPB-RhH**, the two catalysts reaching however the same maximum TON of ca. 8300 after 24 hours (Figure S57).

To get insight into the evolution of the molecular Rh active site within the MOF, diffuse reflectance infrared Fourier transform (DRIFT) spectroscopy and PDF analysis, in combination with computational models as structural references, evidenced that the two catalysts from the two Rh precursors showed similar spectroscopic fingerprints after exposure to $CO/H_2/C_2H_4$ mixture.

In the case of **MOF-808-2.0DPPB-RhH**, DRIFT spectroscopy, performed under a $CO/H_2/C_2H_4$ gas stream at atmospheric pressure and 70°C, showed two strong signals at 2080 and 2009 $cm^{-1}$ (Fig. S73) which were attributed to geminal-dicarbonyls at the rhodium atom as previously reported for homogeneous Rh-P catalytic intermediate.[70] The signal due to adsorbed hydrocarbons was essentially nil. After removal of CO from the gas feed, the signal at 2080 $cm^{-1}$ was found to slowly vanish while the signal at 2009 $cm^{-1}$ was shifted to 2017 $cm^{-1,}$ and no CH signal was formed. We concluded that ethylene was reacting with one of the two geminal CO-Rh, with an initial TOF of *ca.* 4.7 $h^{-1}$ (Figure S74, Left) and that no product accumulated at the surface. The same geminal-dicarbonyl signal was almost instantly recovered when CO was reintroduced in the feed.[71] These data show that CO adsorbed much more strongly than ethylene, which probably reacted from the gas-phase (or a weakly bound state) with one of the CO from the rhodium geminal-dicarbonyl species to form the reaction product that readily desorbed. This process is in line with the reported first catalytic steps for molecular Rh-catalyzed hydroformylation.[72] The TOF measured in the DRIFTS experiment is smaller than that reported in Table 2, as lower temperatures (70 °C instead of 110 °C) and pressures (1 bar instead of 20 bars) were used.

In the case of **MOF-808-2.0DPPB-Rh**, the Rh(acac) cannot be considered as a catalytically active species, in contrast to RhH, according to reported hydroformylation catalytic mechanism.[60,61] Thus, under gas mixture stream at 1 bar and 70°C, the removal of the acac group took place leading to Rh gem-dicarbonyl species similar to those observed for the **MOF-808-2.0DPPB-RhH**. This species then reacts similarly with ethylene as in the case of the RhH precursor, with somewhat lower TOF (2.0 $h^{-1}$) (see Figure S74, Right).

Similarly, the PDF analysis performed on **MOF-808-2.0DPPB-RhH** catalyst showed that the experimental *G(r)* curve remains the same at long-range order before and after catalysis, highlighting the stability of the MOF framework. On the short range, slight changes are observed involving the shoulder at 2.75 Å, previously assigned to the P-C distance. Those changes might evidence the evolution from the catalyst precursor to the Rh active species within the MOF. Also, on the short range no changes of interatomic distances attributed to the host occur, demonstrating the integrity of the $Zr_6$ nodes. In contrast, more significant changes in **MOF-808-2.0DPPB-Rh** experimental *G(r)* curves, before and after catalysis, showed that the Rh(acac) precursor, as well as the $Zr_6$ nodes, slightly evolved during catalysis to give the same structure after catalysis than that obtained for **MOF-808-2.0DPPB-RhH** (Figure S78). Thus, under catalytic conditions, the two MOF catalysts seem converging towards the same structure, more likely based on a phosphine rhodium hydrido intermediate as expected from reaction mechanism.[60,61]

From the experimental catalytic activities at 10 and 20 bars reported on Figure 4, the apparent energy of activation was calculated to be very similar for the two catalysts, with 30 kJ/mol for **MOF-808-2.0DPPB-RhH** and 32 kJ/mol for **MOF-808-2.0DPPB-Rh** (Figure S75), in the range of values reported for different rhodium heterogeneous catalysts (27- 56 kJ/mol).[73–75] These rather low values of the apparent activation energy cannot be attributed to internal diffusion limitations. Indeed the Weisz modulus, defined to estimate the influence of pore diffusion on reaction rates in heterogeneous catalytic reactions,[76] was calculated to be $3{\cdot}10^{-5}$, using a conservative value for the diffusion coefficient of alkanes in MOFs of $1{\cdot}10^{-9}$ $m^2/s$.[77] This value indicates a catalyst effectiveness factor of 1 meaning that the reaction takes place into the whole catalyst particle.

**MOF-catalyzed hydroformylation of higher alkenes.** The absence of diffusion limitation within the **MOF-808-2.0DPPB-RhH** catalyst was further evidenced by the use of longer chain and bulkier alkenes as catalysis substrates. 1-Hexene, 1-decene, 1-dodecene and styrene were all efficiently converted into the corresponding aldehydes through hydroformylation at 110°C under 20 bars of a 1:1 $CO:H_2$ mixture in toluene (Table S4). The **MOF-808-2.0DPPB-RhH** allowed reaching similar yields and selectivity of linear vs branched aldehydes after 3 hours compared to the homogeneous $RhH(CO)(PPh_3)_3$ analogous catalyst. Isomerization was observed for all the alkenes tested. For long chain 1-decene and 1-dodecene, the yield was slightly lower but the selectivity in branched aldehydes slightly higher with the **MOF-808-2.0DPPB-RhH** ($C_{10}$: TON = 420, branched:linear = 1.5; $C_{12}$: TON = 445, branched:linear = 2.3) compared to the molecular homogeneous $RhH(CO)(PPh_3)_3$ ($C_{10}$: TON = 475, branched:linear = 1.35; $C_{12}$: TON = 519, branched:linear = 1.7), more likely due to possible isomerization at the MOF node.[78]

## CONCLUSION

We exploited the unique features of MOF materials to efficiently assemble molecular catalysts on a heterogeneous fashion following a stepwise methodology based on molecular chemistry principles. The ability of MOF-808 to undergo carboxylate ligand substitution allowed for the grafting of dangling phosphine groups, analogous to triphenylphosphines, without significant oxidation. The subsequent coordination with molecular rhodium complexes, using either hydrido or acetylacetonato precursors, gave rise to the heterogenization of organometallic P-Rh(CO) catalysts whose molecular nature was preserved within the porosity of the MOF. The obtained Rh-functionalized MOF were shown to heterogeneously catalyze the hydroformylation of ethylene towards propionaldehyde selectively under triphasic batch conditions. The best catalyst **MOF-808-2.0DPPB-RhH** showed a TOF of 2114 $h^{-1}$ and a TON of 6342 under 20 bars of a mixture $C_2H_4:H_2:CO$ (1:1:1) at 125 °C.

The same MOF catalysts was also stable after recycling. The same catalyst was also found to efficiently catalyze the hydroformylation of $C_6$ to $C_{12}$ linear alkenes and styrene with the same activity than its molecular homogenous analogue. Experimental kinetic data and PDF analysis supported by classical and DFT-level calculations allowed unravelling the atomic-level structure of the active site. Together, calculations and experimental data unraveled the evolution of the two Rh precursors within the MOF converging towards the same type of active species upon catalysis. Furthermore, the MOF-heterogenized catalyst followed the same reaction mechanisms than its homogeneous counterparts with a possible stabilization arising from neighboring ligands confined in the MOF's pore and without diffusion limitation. Thus MOF, conceived as porous solid macroligands in molecular complexes, allow for the access of both the ultrafine knowledge of molecular catalysis and the operability of heterogeneous catalysis.

## AUTHOR INFORMATION

### Corresponding Author

**Jérôme Canivet** – Univ. Lyon, Université Claude Bernard Lyon 1, CNRS, IRCELYON - UMR 5256, 69626 Villeurbanne, France; orcid.org/0000-0002-0458-3085; Email: jerome.canivet@ircelyon.univ-lyon1.fr

### Author Contributions

The manuscript was written through contributions of all authors. All authors have given approval to the final version of the manuscript.

### Notes

The authors declare no competing financial interest.

## ACKNOWLEDGMENT

This work has been carried out within the C123 project that has received funding from the European Union's Horizon 2020 research and innovation program under Grant Agreement No. 814557. JC and PS are very grateful to C123 partners and in particular to Dr. Richard Heyn (Sintef, Norway) for fruitful discussion. F.M.W. acknowledges funding from DECHEMA (Max-Buchner-Forschungsstiftung 3815). The calculations have been performed using the HPC national resources from GENCI (CINES/TGCC) through 2021 Grant A0090907343. The authors also thank the IRCELYON scientific services.

## REFERENCES

(1) Copéret, C.; Comas-Vives, A.; Conley, M. P.; Estes, D. P.; Fedorov, A.; Mougel, V.; Nagae, H.; Núñez-Zarur, F.; Zhizhko, P. A. Surface Organometallic and Coordination Chemistry toward Single-Site Heterogeneous Catalysts: Strategies, Methods, Structures, and Activities. *Chem. Rev.* **2016**, *116* (2), 323–421. https://doi.org/10.1021/acs.chemrev.5b00373.

(2) Samantaray, M. K.; Pump, E.; Bendjeriou-Sedjerari, A.; D'Elia, V.; Pelletier, J. D. A.; Guidotti, M.; Psaro, R.; Basset, J.-M. Surface Organometallic Chemistry in Heterogeneous Catalysis. *Chem. Soc. Rev.* **2018**, *47* (22), 8403–8437. https://doi.org/10.1039/C8CS00356D.

(3) Samantaray, M. K.; D'Elia, V.; Pump, E.; Falivene, L.; Harb, M.; Ould Chikh, S.; Cavallo, L.; Basset, J.-M. The Comparison between Single Atom Catalysis and Surface Organometallic Catalysis. *Chem. Rev.* **2020**, *120* (2), 734–813. https://doi.org/10.1021/acs.chemrev.9b00238.

(4) Thomas, J. M.; Raja, R. Exploiting Nanospace for Asymmetric Catalysis: Confinement of Immobilized, Single-Site Chiral Catalysts Enhances Enantioselectivity. *Acc. Chem. Res.* **2008**, *41* (6), 708–720. https://doi.org/10.1021/ar700217y.

(5) Hübner, S.; de Vries, J. G.; Farina, V. Why Does Industry Not Use Immobilized Transition Metal Complexes as Catalysts? *Adv. Synth. Catal.* **2016**, *358* (1), 3–25. https://doi.org/10.1002/adsc.201500846.

(6) Witzke, R. J.; Chapovetsky, A.; Conley, M. P.; Kaphan, D. M.; Delferro, M. Nontraditional Catalyst Supports in Surface Organometallic Chemistry. *ACS Catal.* **2020**, *10* (20), 11822–11840. https://doi.org/10.1021/acscatal.0c03350.

(7) Wisser, F. M.; Mohr, Y.; Quadrelli, E. A.; Canivet, J. Porous Macroligands: Materials for Heterogeneous Molecular Catalysis. *ChemCatChem* **2020**, *12* (5), 1270–1275. https://doi.org/10.1002/cctc.201902064.

(8) Kumar, S.; Mohan, B.; Tao, Z.; You, H.; Ren, P. Incorporation of Homogeneous Organometallic Catalysts into Metal–Organic Frameworks for Advanced Heterogenization: A Review. *Catal. Sci. Technol.* **2021**, *11* (17), 5734–5771. https://doi.org/10.1039/D1CY00663K.

(9) Siwaipram, S.; Impeng, S.; Bureekaew, P. A. B. and S. *Density Functional Theory Studies of Catalytic Sites in Metal- Organic Frameworks*; IntechOpen, 2018. https://doi.org/10.5772/intechopen.80698.

(10) Wei, Y.-S.; Zhang, M.; Zou, R.; Xu, Q. Metal–Organic Framework-Based Catalysts with Single Metal Sites. *Chem. Rev.* **2020**, *120* (21), 12089–12174. https://doi.org/10.1021/acs.chemrev.9b00757.

(11) Liu, J.; Ye, J.; Li, Z.; Otake, K.; Liao, Y.; Peters, A. W.; Noh, H.; Truhlar, D. G.; Gagliardi, L.; Cramer, C. J.; Farha, O. K.; Hupp, J. T. Beyond the Active Site: Tuning the Activity and Selectivity of a Metal–Organic Framework-Supported Ni Catalyst for Ethylene Dimerization. *J. Am. Chem. Soc.* **2018**, *140* (36), 11174–11178. https://doi.org/10.1021/jacs.8b06006.

(12) Barona, M.; Ahn, S.; Morris, W.; Hoover, W.; Notestein, J. M.; Farha, O. K.; Snurr, R. Q. Computational Predictions and Experimental Validation of Alkane Oxidative Dehydrogenation by Fe2M MOF Nodes. *ACS Catal.* **2020**, *10* (2), 1460–1469. https://doi.org/10.1021/acscatal.9b03932.

(13) Antil, N.; Kumar, A.; Akhtar, N.; Newar, R.; Begum, W.; Dwivedi, A.; Manna, K. Aluminum Metal–Organic Framework-Ligated Single-Site Nickel(II)-Hydride for Heterogeneous Chemoselective Catalysis. *ACS Catal.* **2021**, *11* (7), 3943–3957. https://doi.org/10.1021/acscatal.0c04379.

(14) Antil, N.; Kumar, A.; Akhtar, N.; Newar, R.; Begum, W.; Manna, K. Metal–Organic Framework-Confined Single-Site Base-Metal Catalyst for Chemoselective Hydrodeoxygenation of Carbonyls and Alcohols. *Inorg. Chem.* **2021**, *60* (12), 9029–9039. https://doi.org/10.1021/acs.inorgchem.1c01008.

(15) Antil, N.; Kumar, A.; Akhtar, N.; Begum, W.; Chauhan, M.; Newar, R.; Rawat, M. S.; Manna, K. Chemoselective and Tandem Reduction of Arenes Using a Metal–Organic Framework-Supported Single-Site Cobalt Catalyst. *Inorg. Chem.* **2022**, *61* (2), 1031–1040. https://doi.org/10.1021/acs.inorgchem.1c03098.

(16) Chen, C.; Alalouni, M. R.; Dong, X.; Cao, Z.; Cheng, Q.; Zheng, L.; Meng, L.; Guan, C.; Liu, L.; Abou-Hamad, E.; Wang, J.; Shi, Z.; Huang, K.-W.; Cavallo, L.; Han, Y. Highly Active Heterogeneous Catalyst for Ethylene Dimerization Prepared by Selectively Doping Ni on the Surface of a Zeolitic Imidazolate Framework. *J. Am. Chem. Soc.* **2021**, *143* (18), 7144–7153. https://doi.org/10.1021/jacs.1c02272.

(17) Yeh, B.; Vicchio, S. P.; Chheda, S.; Zheng, J.; Schmid, J.; Löbbert, L.; Bermejo-Deval, R.; Gutiérrez, O. Y.; Lercher, J. A.; Lu, C. C.; Neurock, M.; Getman, R. B.; Gagliardi, L.; Bhan, A. Site Densities, Rates, and Mechanism of Stable Ni/UiO-66 Ethylene Oligomerization Catalysts. *J. Am. Chem. Soc.* **2021**, *143* (48), 20274–20280. https://doi.org/10.1021/jacs.1c09320.

(18) Platero-Prats, A. E.; Mavrandonakis, A.; Liu, J.; Chen, Z.; Chen, Z.; Li, Z.; Yakovenko, A. A.; Gallington, L. C.; Hupp, J. T.; Farha, O. K.; Cramer, C. J.; Chapman, K. W. The Molecular Path Approaching the Active Site in Catalytic Metal–Organic Frameworks. *J. Am. Chem. Soc.* **2021**, *143* (48), 20090–20094. https://doi.org/10.1021/jacs.1c11213.

(19) Canivet, J.; Bernoud, E.; Bonnefoy, J.; Legrand, A.; Todorova, T. K.; Quadrelli, E. A.; Mellot-Draznieks, C. Synthetic and Computational Assessment of a Chiral Metal–Organic Framework Catalyst for Predictive Asymmetric Transformation. *Chem. Sci.* **2020**, *11* (33), 8800–8808. https://doi.org/10.1039/D0SC03364B.

(20) Gillespie, J. A.; Zuidema, E.; van Leeuwen, P. W. N. M.; Kamer, P. C. J. Phosphorus Ligand Effects in Homogeneous Catalysis and Rational Catalyst Design. In *Phosphorus(III) Ligands in Homogeneous Catalysis: Design and Synthesis*; John Wiley & Sons, Ltd; pp 1–26. https://doi.org/10.1002/9781118299715.ch1.

(21) Clevenger, A. L.; Stolley, R. M.; Aderibigbe, J.; Louie, J. Trends in the Usage of Bidentate Phosphines as Ligands in Nickel Catalysis. *Chem. Rev.* **2020**, *120* (13), 6124–6196. https://doi.org/10.1021/acs.chemrev.9b00682.

(22) Oser, W. R. M.; Papile, C. J.; Weininger, S. J. Mechanism of Deactivation in Phosphine-Modified Rhodium-Catalyzed Hydroformylation: A CIR-FTIR Study. *J. Mol. Catal.* **1987**, *41* (3), 293–302. https://doi.org/10.1016/0304-5102(87)80107-4.

(23) Pascanu, V.; González Miera, G.; Inge, A. K.; Martín-Matute, B. Metal–Organic Frameworks as Catalysts for Organic Synthesis: A Critical Perspective. *J. Am. Chem. Soc.* **2019**, *141* (18), 7223–7234. https://doi.org/10.1021/jacs.9b00733.

(24) Dhakshinamoorthy, A.; Asiri, A. M.; Garcia, H. Catalysis in Confined Spaces of Metal Organic Frameworks. *ChemCatChem* **2020**, *12* (19), 4732–4753. https://doi.org/10.1002/cctc.202001188.

(25) Liu, J.; Goetjen, T. A.; Wang, Q.; Knapp, J. G.; Wasson, M. C.; Yang, Y.; Syed, Z. H.; Delferro, M.; Notestein, J. M.; Farha, O. K.; Hupp, J. T. MOF-Enabled Confinement and Related Effects for Chemical Catalyst Presentation and Utilization. *Chem. Soc. Rev.* **2022**. https://doi.org/10.1039/D1CS00968K.

(26) Orton, G. R. F.; Pilgrim, B. S.; Champness, N. R. The Chemistry of Phosphines in Constrained, Well-Defined Microenvironments. *Chem. Soc. Rev.* **2021**, *50* (7), 4411–4431. https://doi.org/10.1039/D0CS01556C.

(27) Newar, R.; Begum, W.; Akhtar, N.; Antil, N.; Chauhan, M.; Kumar, A.; Gupta, P.; Malik, J.; Balendra; Manna, K. Mono-Phosphine Metal-Organic Framework-Supported Cobalt Catalyst for Efficient Borylation Reactions. *Eur. J. Inorg. Chem.* **2022**, *2022* (10), e202101019. https://doi.org/10.1002/ejic.202101019.

(28) Morel, F. L.; Ranocchiari, M.; van Bokhoven, J. A. Synthesis and Characterization of Phosphine-Functionalized Metal–Organic Frameworks Based on MOF-5 and MIL-101 Topologies. *Ind. Eng. Chem. Res.* **2014**, *53* (22), 9120–9127. https://doi.org/10.1021/ie403549v.

(29) Xu, X.; Rummelt, S. M.; Morel, F. L.; Ranocchiari, M.; van Bokhoven, J. A. Selective Catalytic Behavior of a Phosphine-Tagged Metal-Organic Framework Organocatalyst. *Chem. – Eur. J.* **2014**, *20* (47), 15467–15472. https://doi.org/10.1002/chem.201404498.

(30) Morel, F. L.; Pin, S.; Huthwelker, T.; Ranocchiari, M.; Bokhoven, J. A. van. Phosphine and Phosphine Oxide Groups in Metal–Organic Frameworks Detected by P K-Edge XAS. *Phys. Chem. Chem. Phys.* **2015**, *17* (5), 3326–3331. https://doi.org/10.1039/C4CP05151C.

(31) Sawano, T.; Lin, Z.; Boures, D.; An, B.; Wang, C.; Lin, W. Metal–Organic Frameworks Stabilize Mono(Phosphine)–Metal Complexes for Broad-Scope Catalytic Reactions. *J. Am. Chem. Soc.* **2016**, *138* (31), 9783–9786. https://doi.org/10.1021/jacs.6b06239.

(32) Falkowski, J. M.; Sawano, T.; Zhang, T.; Tsun, G.; Chen, Y.; Lockard, J. V.; Lin, W. Privileged Phosphine-Based Metal–Organic Frameworks for Broad-Scope Asymmetric Catalysis. *J. Am. Chem. Soc.* **2014**, *136* (14), 5213–5216. https://doi.org/10.1021/ja500090y.

(33) Dunning, S. G.; Nandra, G.; Conn, A. D.; Chai, W.; Sikma, R. E.; Lee, J. S.; Kunal, P.; Reynolds III, J. E.; Chang, J.-S.; Steiner, A.; Henkelman, G.; Humphrey, S. M. A Metal–Organic Framework with Cooperative Phosphines That Permit Post-Synthetic Installation of Open Metal Sites. *Angew. Chem. Int. Ed.* **2018**, *57* (30), 9295–9299. https://doi.org/10.1002/anie.201802402.

(34) Wen, Y.; Zhang, J.; Xu, Q.; Wu, X.-T.; Zhu, Q.-L. Pore Surface Engineering of Metal–Organic Frameworks for Heterogeneous Catalysis. *Coord. Chem. Rev.* **2018**, *376*, 248–276. https://doi.org/10.1016/j.ccr.2018.08.012.

(35) Chen, Z.; Hanna, S. L.; Redfern, L. R.; Alezi, D.; Islamoglu, T.; Farha, O. K. Reticular Chemistry in the Rational Synthesis of Functional Zirconium Cluster-Based MOFs. *Coord. Chem. Rev.* **2019**, *386*, 32–49. https://doi.org/10.1016/j.ccr.2019.01.017.

(36) Yin, Z.; Wan, S.; Yang, J.; Kurmoo, M.; Zeng, M.-H. Recent Advances in Post-Synthetic Modification of Metal–Organic Frameworks: New Types and Tandem Reactions. *Coord. Chem. Rev.* **2019**, *378*, 500–512. https://doi.org/10.1016/j.ccr.2017.11.015.

(37) Prasad, R. R. R.; Dawson, D. M.; Cox, P. A.; Ashbrook, S. E.; Wright, P. A.; Clarke, M. L. A Bifunctional MOF Catalyst Containing Metal–Phosphine and Lewis Acidic Active Sites. *Chem. – Eur. J.* **2018**, *24* (57), 15309–15318. https://doi.org/10.1002/chem.201803094.

(38) Van Vu, T.; Kosslick, H.; Schulz, A.; Harloff, J.; Paetzold, E.; Schneider, M.; Radnik, J.; Steinfeldt, N.; Fulda, G.; Kragl, U. Selective Hydroformylation of Olefins over the Rhodium Supported Large Porous Metal–Organic Framework MIL-101. *Appl. Catal. Gen.* **2013**, *468*, 410–417. https://doi.org/10.1016/j.apcata.2013.09.011.

(39) Van Vu, T.; Kosslick, H.; Schulz, A.; Harloff, J.; Paetzold, E.; Radnik, J.; Kragl, U.; Fulda, G.; Janiak, C.;

Tuyen, N. D. Hydroformylation of Olefins over Rhodium Supported Metal-Organic Framework Catalysts of Different Structure. *Microporous Mesoporous Mater.* **2013**, *177*, 135–142. https://doi.org/10.1016/j.micromeso.2013.02.035.

(40) Hou, C.; Zhao, G.; Ji, Y.; Niu, Z.; Wang, D.; Li, Y. Hydroformylation of Alkenes over Rhodium Supported on the Metal-Organic Framework ZIF-8. *Nano Res.* **2014**, *7* (9), 1364–1369. https://doi.org/10.1007/s12274-014-0501-4.

(41) Sartipi, S.; Valero Romero, M. J.; Rozhko, E.; Que, Z.; Stil, H. A.; de With, J.; Kapteijn, F.; Gascon, J. Dynamic Release–Immobilization of a Homogeneous Rhodium Hydroformylation Catalyst by a Polyoxometalate Metal–Organic Framework Composite. *ChemCatChem* **2015**, *7* (20), 3243–3247. https://doi.org/10.1002/cctc.201500330.

(42) Vu, T. V.; Kosslick, H.; Schulz, A.; Harloff, J.; Paetzold, E.; Lund, H.; Kragl, U.; Schneider, M.; Fulda, G. Influence of the Textural Properties of Rh/MOF-5 on the Catalytic Properties in the Hydroformylation of Olefins. *Microporous Mesoporous Mater.* **2012**, *154*, 100–106. https://doi.org/10.1016/j.micromeso.2011.11.052.

(43) Tang, P.; Paganelli, S.; Carraro, F.; Blanco, M.; Riccò, R.; Marega, C.; Badocco, D.; Pastore, P.; Doonan, C. J.; Agnoli, S. Postsynthetic Metalated MOFs as Atomically Dispersed Catalysts for Hydroformylation Reactions. *ACS Appl. Mater. Interfaces* **2020**, *12* (49), 54798–54805. https://doi.org/10.1021/acsami.0c17073.

(44) Furukawa, H.; Gándara, F.; Zhang, Y.-B.; Jiang, J.; Queen, W. L.; Hudson, M. R.; Yaghi, O. M. Water Adsorption in Porous Metal–Organic Frameworks and Related Materials. *J. Am. Chem. Soc.* **2014**, *136* (11), 4369–4381. https://doi.org/10.1021/ja500330a.

(45) Ly, H. G. T.; Fu, G.; Kondinski, A.; Bueken, B.; De Vos, D.; Parac-Vogt, T. N. Superactivity of MOF-808 toward Peptide Bond Hydrolysis. *J. Am. Chem. Soc.* **2018**, *140* (20), 6325–6335. https://doi.org/10.1021/jacs.8b01902.

(46) Dai, S.; Simms, C.; Dovgaliuk, I.; Patriarche, G.; Tissot, A.; Parac-Vogt, T. N.; Serre, C. Monodispersed MOF-808 Nanocrystals Synthesized via a Scalable Room-Temperature Approach for Efficient Heterogeneous Peptide Bond Hydrolysis. *Chem. Mater.* **2021**, *33* (17), 7057–7066. https://doi.org/10.1021/acs.chemmater.1c02174.

(47) Hardian, R.; Dissegna, S.; Ullrich, A.; Llewellyn, P. L.; Coulet, M.-V.; Fischer, R. A. Tuning the Properties of MOF-808 via Defect Engineering and Metal Nanoparticle Encapsulation. *Chem. – Eur. J.* **2021**, *27* (22), 6804–6814. https://doi.org/10.1002/chem.202005050.

(48) Lyu, H.; Chen, O. I.-F.; Hanikel, N.; Hossain, M. I.; Flaig, R. W.; Pei, X.; Amin, A.; Doherty, M. D.; Impastato, R. K.; Glover, T. G.; Moore, D. R.; Yaghi, O. M. Carbon Dioxide Capture Chemistry of Amino Acid Functionalized Metal–Organic Frameworks in Humid Flue Gas. *J. Am. Chem. Soc.* **2022**, *144* (5), 2387–2396. https://doi.org/10.1021/jacs.1c13368.

(49) Baek, J.; Rungtaweevoranit, B.; Pei, X.; Park, M.; Fakra, S. C.; Liu, Y.-S.; Matheu, R.; Alshmimri, S. A.; Alshehri, S.; Trickett, C. A.; Somorjai, G. A.; Yaghi, O. M. Bioinspired Metal–Organic Framework Catalysts for Selective Methane Oxidation to Methanol. *J. Am. Chem. Soc.* **2018**, *140* (51), 18208–18216. https://doi.org/10.1021/jacs.8b11525.

(50) Velthoven, N. V.; Waitschat, S.; Chavan, S. M.; Liu, P.; Smolders, S.; Vercammen, J.; Bueken, B.; Bals, S.; Lillerud, K. P.; Stock, N.; Vos, D. E. D. Single-Site Metal–Organic Framework Catalysts for the Oxidative Coupling of Arenes via C–H/C–H Activation. *Chem. Sci.* **2019**, *10* (12), 3616–3622. https://doi.org/10.1039/C8SC05510F.

(51) Karmakar, S.; Barman, S.; Rahimi, F. A.; Maji, T. K. Covalent Grafting of Molecular Photosensitizer and Catalyst on MOF-808: Effect of Pore Confinement toward Visible Light-Driven CO2 Reduction in Water. *Energy Environ. Sci.* **2021**, *14* (4), 2429–2440. https://doi.org/10.1039/D0EE03643A.

(52) Pruett, R. L.; Smith, J. A. Low-Pressure System for Producing Normal Aldehydes by Hydroformylation of .Alpha.-Olefins. *J. Org. Chem.* **1969**, *34* (2), 327–330. https://doi.org/10.1021/jo01254a015.

(53) Bennett, T. D.; Cheetham, A. K. Amorphous Metal–Organic Frameworks. *Acc. Chem. Res.* **2014**, *47* (5), 1555–1562. https://doi.org/10.1021/ar5000314.

(54) Benseghir, Y.; Lemarchand, A.; Duguet, M.; Mialane, P.; Gomez-Mingot, M.; Roch-Marchal, C.; Pino, T.; Ha-Thi, M.-H.; Haouas, M.; Fontecave, M.; Dolbecq, A.; Sassoye, C.; Mellot-Draznieks, C. Co-Immobilization of a Rh Catalyst and a Keggin Polyoxometalate in the UiO-67 Zr-Based Metal–Organic Framework: In Depth Structural Characterization and Photocatalytic Properties for CO 2 Reduction. *J. Am. Chem. Soc.* **2020**, *142* (20), 9428–9438. https://doi.org/10.1021/jacs.0c02425.

(55) Ghosh, A. C.; Legrand, A.; Rajapaksha, R.; Craig, G. A.; Sassoye, C.; Balázs, G.; Farrusseng, D.; Furukawa, S.; Canivet, J.; Wisser, F. M. Rhodium-Based Metal–Organic Polyhedra Assemblies for Selective CO2 Photoreduction. *J. Am. Chem. Soc.* **2022**, *144* (8), 3626–3636. https://doi.org/10.1021/jacs.1c12631.

(56) Romero-Muñiz, I.; Romero-Muñiz, C.; del Castillo-Velilla, I.; Marini, C.; Calero, S.; Zamora, F.; Platero-Prats, A. E. Revisiting Vibrational Spectroscopy to Tackle the Chemistry of Zr6O8 Metal-Organic Framework Nodes. *ACS Appl. Mater. Interfaces* **2022**, *14* (23), 27040–27047. https://doi.org/10.1021/acsami.2c04712.

(57) Ortiz-Espinoza, A. P.; Noureldin, M. M. B.; El-Halwagi, M. M.; Jiménez-Gutiérrez, A. Design, Simulation and Techno-Economic Analysis of Two Processes for the Conversion of Shale Gas to Ethylene. *Comput. Chem. Eng.* **2017**, *107*, 237–246. https://doi.org/10.1016/j.compchemeng.2017.05.023.

(58) Mohsenzadeh, A.; Zamani, A.; Taherzadeh, M. J. Bioethylene Production from Ethanol: A Review and Techno-Economical Evaluation. *ChemBioEng Rev.* **2017**, *4* (2), 75–91. https://doi.org/10.1002/cben.201600025.

(59) Phung, T. K.; Pham, T. L. M.; Vu, K. B.; Busca, G. (Bio)Propylene Production Processes: A Critical Review. *J. Environ. Chem. Eng.* **2021**, *9* (4), 105673. https://doi.org/10.1016/j.jece.2021.105673.

(60) How, R. C.; Hembre, R.; Ponasik, J. A.; Tolleson, G. S.; Clarke, M. L. A Modular Family of Phosphine-Phosphoramidite Ligands and Their Hydroformylation Catalysts: Steric Tuning Impacts upon the Coordination Geometry of Trigonal Bipyramidal Complexes of Type [Rh(H)(CO)2(P^P*)]. *Catal. Sci. Technol.* **2015**, *6* (1), 118–124. https://doi.org/10.1039/C5CY00886G.

(61) Jacobs, I.; de Bruin, B.; Reek, J. N. H. Comparison of the Full Catalytic Cycle of Hydroformylation Mediated by

Mono- and Bis-Ligated Triphenylphosphine–Rhodium Complexes by Using DFT Calculations. *ChemCatChem* **2015**, *7* (11), 1708–1718. https://doi.org/10.1002/cctc.201500087.

(62) Walczuk, E. B.; Kamer, P. C. J.; van Leeuwen, P. W. N. M. Dormant States of Rhodium Hydroformylation Catalysts: Carboalkoxyrhodium Complex Formed from Enones in the Alkene Feed. *Angew. Chem. Int. Ed.* **2003**, *42* (38), 4665–4669. https://doi.org/10.1002/anie.200351884.

(63) Köhnke, K.; Wessel, N.; Esteban, J.; Jin, J.; Vorholt, A. J.; Leitner, W. Operando Monitoring of Mechanisms and Deactivation of Molecular Catalysts. *Green Chem.* **2022**, *24* (5), 1951–1972. https://doi.org/10.1039/D1GC04383H.

(64) Zeelie, T. A.; Root, A.; Krause, A. O. I. Rh/Fibre Catalyst for Ethene Hydroformylation: Catalytic Activity and Characterisation. *Appl. Catal. Gen.* **2005**, *285* (1), 96–109. https://doi.org/10.1016/j.apcata.2005.02.010.

(65) Jiang, M.; Yan, L.; Ding, Y.; Sun, Q.; Liu, J.; Zhu, H.; Lin, R.; Xiao, F.; Jiang, Z.; Liu, J. Ultrastable 3V-PPh3 Polymers Supported Single Rh Sites for Fixed-Bed Hydroformylation of Olefins. *J. Mol. Catal. Chem.* **2015**, *404–405*, 211–217. https://doi.org/10.1016/j.molcata.2015.05.008.

(66) Dhainaut, J.; Avci-Camur, C.; Troyano, J.; Legrand, A.; Canivet, J.; Imaz, I.; Maspoch, D.; Reinsch, H.; Farrusseng, D. Systematic Study of the Impact of MOF Densification into Tablets on Textural and Mechanical Properties. *CrystEngComm* **2017**, *19* (29), 4211–4218. https://doi.org/10.1039/C7CE00338B.

(67) Poloneeva, D.; Datta, S. J.; Garzon-Tovar, L.; Durini, S.; Rueping, M.; Eddaoudi, M.; Bavykina, A.; Gascon, J. Toward Liquid Phase Processable Metal Organic Frameworks: Dream or Reality? *Acc. Mater. Res.* **2021**, *2* (12), 1133–1140. https://doi.org/10.1021/accountsmr.1c00100.

(68) Yeskendir, B.; Dacquin, J.-P.; Lorgouilloux, Y.; Courtois, C.; Royer, S.; Dhainaut, J. From Metal–Organic Framework Powders to Shaped Solids: Recent Developments and Challenges. *Mater. Adv.* **2021**, *2* (22), 7139–7186. https://doi.org/10.1039/D1MA00630D.

(69) Wang, T. C.; Wright, A. M.; Hoover, W. J.; Stoffel, K. J.; Richardson, R. K.; Rodriguez, S.; Flores, R. C.; Siegfried, J. P.; Vermeulen, N. A.; Fuller, P. E.; Weston, M. H.; Farha, O. K.; Morris, W. Surviving Under Pressure: The Role of Solvent, Crystal Size, and Morphology During Pelletization of Metal–Organic Frameworks. *ACS Appl. Mater. Interfaces* **2021**, *13* (44), 52106–52112. https://doi.org/10.1021/acsami.1c09619.

(70) Matsubu, J. C.; Yang, V. N.; Christopher, P. Isolated Metal Active Site Concentration and Stability Control Catalytic CO2 Reduction Selectivity. *J. Am. Chem. Soc.* **2015**, *137* (8), 3076–3084. https://doi.org/10.1021/ja5128133.

(71) Martinez-Macias, C.; Serna, P.; Gates, B. C. Isostructural Zeolite-Supported Rhodium and Iridium Complexes: Tuning Catalytic Activity and Selectivity by Ligand Modification. *ACS Catal.* **2015**, *5* (10), 5647–5656. https://doi.org/10.1021/acscatal.5b00995.

(72) Moser, W. R.; Papile, C. J.; Brannon, D. A.; Duwell, R. A.; Weininger, S. J. The Mechanism of Phosphine-Modified Rhodium-Catalyzed Hydroformylation Studied by CIR-FTIR. *J. Mol. Catal.* **1987**, *41* (3), 271–292. https://doi.org/10.1016/0304-5102(87)80106-2.

(73) Arai, H.; Tominaga, H. Hydroformylation and Hydrogenation of Olefins over Rhodium Zeolite Catalyst. *J. Catal.* **1982**, *75* (1), 188–189. https://doi.org/10.1016/0021-9517(82)90134-8.

(74) Takahashi, N.; Kobayashi, M. Comparison of Ethylene with Propylene Hydroformylation over a Rh-Y Zeolite Catalyst under Atmospheric Pressure. *J. Catal.* **1984**, *85* (1), 89–97. https://doi.org/10.1016/0021-9517(84)90112-X.

(75) Ro, I.; Xu, M.; Graham, G. W.; Pan, X.; Christopher, P. Synthesis of Heteroatom Rh–ReOx Atomically Dispersed Species on Al2O3 and Their Tunable Catalytic Reactivity in Ethylene Hydroformylation. *ACS Catal.* **2019**, *9* (12), 10899–10912. https://doi.org/10.1021/acscatal.9b02111.

(76) Weisz, P. B.; Prater, C. D. Interpretation of Measurements in Experimental Catalysis. In *Advances in Catalysis*; Frankenburg, W. G., Komarewsky, V. I., Rideal, E. K., Eds.; Academic Press, 1954; Vol. 6, pp 143–196. https://doi.org/10.1016/S0360-0564(08)60390-9.

(77) Stallmach, F.; Gröger, S.; Künzel, V.; Kärger, J.; Yaghi, O. M.; Hesse, M.; Müller, U. NMR Studies on the Diffusion of Hydrocarbons on the Metal-Organic Framework Material MOF-5. *Angew. Chem. Int. Ed.* **2006**, *45* (13), 2123–2126. https://doi.org/10.1002/anie.200502553.

(78) Hicks, K. E.; Rosen, A. S.; Syed, Z. H.; Snurr, R. Q.; Farha, O. K.; Notestein, J. M. Zr6O8 Node-Catalyzed Butene Hydrogenation and Isomerization in the Metal–Organic Framework NU-1000. *ACS Catal.* **2020**, *10* (24), 14959–14970. https://doi.org/10.1021/acscatal.0c03579.

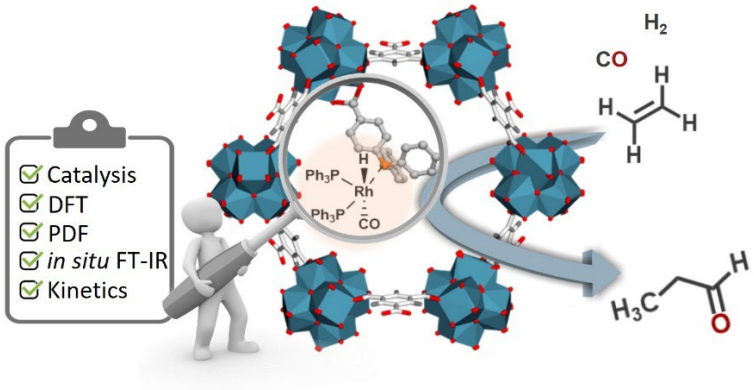
Catalysis
DFT
PDF
in situ FT-IR
Kinetics
H2
CO
Ph3P
Rh
Ph3P
CO
H3C
O